R - 890

DYNAMIC TESTING OF THE KEARFOTT 2401 ACCELEROMETER

by

Bert Katz

June 1975

The Charles Stark Draper Laboratory, Inc.

Cambridge, Massachusetts 02139

R-890

DYNAMIC TESTING OF THE KEARFOTT 2401 ACCELEROMETER

by

Bert Katz

June 1975

THE CHARLES STARK DRAPER LABORATORY INC.

CAMBRIDGE, MASS

02139

ACKNOWLEDGEMENTS

This report was prepared by the Charles Stark Draper Laboratory under Contract NAS8-30255 for the George C. Marshall Space Flight Center of the National Aeronautics and Space Administration.

The work reported herein is a continuation of the effort to conduct dynamic performance tests on a variety of inertial instruments. This effort is being sponsored by NASA-George C. Marshall Space Flight Center.

I would like to express special appreciation to George Bukow for his guidance, technical supervision and substantial inputs which contributed greatly to the successful conclusion of this effort and in the preparation of the final report.

Thanks are also due to the many people in this laboratory who contributed to this report and the work it represents.

Al Moore, laboratory technician, deserves special commendation for the test support.

In the preparation of the Final Report, the contributions of Stephen Hellant in editing and preparation of the document

for publication are appreciated.

The efforts of Linda Willy in preparing the technical illustrations and Jean Pennick in preparing the text input to the computer are also acknowledged and appreciated.

Jerold Gilmore, Division Leader, has technical responsibility for this contract. His supervisory support of all the work is gratefully acknowledged.

DYNAMIC TESTING OF THE KEARFOTT C702401030 ACCELEROMETER

ABSTRACT

A Kearfott C702401030 pendulous accelerometer serial #N3 was integrated with a United Aircraft Pulse Torque Servo Assembly (PTSA) forced binary loop. The test objective was to measure dynamic errors due to anisoinertia and OA coupling effects. The instrument and its torque loop are described and the technique for isolating the anisoinertia error from centripetal acceleration effects is discussed in detail.

The measured anisoinertia error coefficient was 3.0 cm, and the testing confirmed that no rectified OA coupling error was present.

TABLE OF CONTENTS

SECTION 1

INTRODUCTION

This report presents and discusses the results of tests performed on the Singer Kearfott C702401030 pendulous, pulse torqued accelerometer, serial number N3 (hereafter called Kearfott 2401 accelerometer), in a dynamic environment. The accelerometer was tested with a United Aircraft pulse torque servo assembly (PTSA) forced binary loop.

In stabilized platform applications, the various dynamic error sources are not routinely considered since the platform functions to isolate the instruments from undesired dynamic forcing functions. However, in strapdown applications the instruments encounter the full dynamic environment and all error sources must be considered.

The objective of the test program was to investigate and evaluate the accelerometer's dynamic characteristics, specificly, anisoinertia and OA coupling, when the instrument is subjected to angular oscillations and constant rate inputs.

These tests were part of a continuing study program to fully determine expected strapdown system performance in an

angular dynamic environment. It is hoped that the test results observed will aid the strapdown system designer, since little data is currently available for body mounted accelerometers in a dynamic environment.

The report is divided into seven sections and an appendix. A detailed description and performance characteristics of the Kearfott 2401 accelerometer are presented in Section 2. The pulse-torque rebalance loop used in conjunction with the accelerometer, the United Aircraft PTSA, is described in Section 3.

Section 4 provides an introduction and background treatment of the accelerometer dynamic error sources covered in the test program. The output axis dynamic equation is given, and the discussion continues with a detailed description of the anisoinertia and OA coupling dynamic error terms.

The dynamic test facility and test procedures are described in Section 5. A description of the results of the tests run on the accelerometer, together with the approaches used and difficulties encountered, follow in Section 6.

Section 7 presents the conclusions of the dynamic test program and makes recommendations for further investigation of other dynamic error terms, such as sculling, vibropendulosity, and anisoelasticity. These effects are described in detail in

Appendix A together with a test plan for multi-axis oscillatory inputs.

The results and conclusions of this report are based upon a sequence of evaluation tests performed on one instrument. They do not attempt to categorize the Kearfott 2401 accelerometer family.

SECTION 2

INSTRUMENT DESCRIPTION

THE KEARFOTT 2401 ACCELEROMETER

The Kearfott 2401 accelerometer is a single axis, viscous damped, linear device which uses a hinged pendulum as the sensing element. Fig 2.1* shows its outer case dimensions and Table 2.1* lists the operational and performance parameters as quoted by Singer-Kearfott. (Publishing of this performance data in this report does not infer CSDL verification except as indicated in the text.) The pendulum contains both pickoff excitation and DC torquer coils wound on a common form. It is anchored to an aluminum housing through a low creep, low hysteresis, frictionless spring suspension. An alternating current excited, air core differential transformer type pickoff produces a voltage due to the relative displacement, resulting from sensed accelerations, between pendulum and housing. When the accelerometer is used with an analog torque rebalance loop, the accelerometer pickoff voltage is amplified, demodulated and fed back to drive the torque generator thus rebalancing the input acceleration.

* All figures and tables are found at the end of the text

The spring suspension utilizes two integrally mounted leaf springs contained in a common plane, but sufficiently spaced to reduce errors from cross axis acceleration to a negligible level. To provide damping and insure satisfactory operation in severe environments, the entire housing is filled with a silicone fluid.

SECTION 3

REBALANCE LOOP DESCRIPTION

THE UNITED AIRCRAFT PTSA

A United Aircraft Corp. (UAC) forced-binary pulse torque-to-balance loop hereafter called PTSA was interfaced to the Kearfott 2401 accelerometer. The PTSA is a pulse width modulated binary loop which provides digitized torquing signals to rebalance the inertial instrument. A block diagram of the loop is shown in Fig. 3.1. The loop consists of four major functional components:

a) amplifier and demodulator

b) quantizer

3) current bridge and driver

d) current regulator

A brief description of the loop follows.

As the accelerometer senses an input, the instrument pickoff generates a voltage which varies in proportion to the displacement of the pendulum from null. This signal is amplified, demodulated and applied to the loop compensation

network. The output of the loop compensation network is then summed with a reference ramp function of limit cycle frequency and amplified prior to its transmittal to the quantizer. The quantizer detects zero crossings of the resultant wave and then furnishes a signal to switch the current in the torquer from plus to minus thus producing a pulse-width modulated wave of limit cycle frequency. With no acceleration input, the zero crossing occurs at the mid-time point of the limit cycle; for maximum plus or minus rate, the zero crossing occurs at the beginning or end of the limit cycle, respectively. The waveform is shown in Fig. 3.2. Thus, the quantizer generates an output waveform whose duty cycle is approximately proportional to the amplitude of its input signal.

The quantized signal is used to drive an H switch (four transistor bridge) which can reverse the current in the accelerometer torquer. There is a maximum of 64 switching points within the 1KHZ limit cycle period. The polarity of current change occurs at the zero crossing in the quantizer, when the next 64KHZ clock pulse occurs. The magnitude of the torquer current is precisely maintained by a current regulator. The net torque current supplied to the instrument is of a polarity required to return the pendulum to its null position. The PTSA loop, therefore, supplies an average value of current over a limit cycle to balance the torque generated by the rate input and maintains a nearly constant torque coil power regardless of accelerometer input-axis rate.

The quantized output is also used to generate the output data. The PTSA readout is a time-modulated pulse train where the number of pulses is a direct measure of the current feedback to the instrument torquer. Each pulse represents an incremental linear velocity of the accelerometer.

SECTION 4

PENDULOUS ACCELEROMETER DYNAMIC ERROR SOURCES

This section provides a theoretical treatment of the pendulous accelerometer dynamic error sources which were measured during the dynamic test program. The analysis is extensively presented in the reference literature and is only briefly summarized here as reference for the data presented in the test results.

The differential equation describing the dynamics of a single-degree-of-freedom pendulous accelerometer in a rotating system may be formulated in terms of angular momentum and the torque applied to the pendulum.

$$\overline{M}_{OA} = \overline{H} \times \overline{W}_{IA} \tag{4.1}$$

where

$\overline{M}_{OA}$ = torque applied to the pendulous float.

$\overline{H}$ = angular momentum of the pendulous float.

$\overline{W}_{IA}$ = angular velocity of the case about the input axis.

Of interest is the output axis dynamic equation which is derived from the above in the various references and restated here.

(4.2)

$$I_{OA}\ddot{\theta} + C_{OA}\dot{\theta} = P\,a_{IRA} + M_{TG} - P\,a_{PRA}\,\theta - I_{OA}\dot{W}_{ORA} + (I_{PA} - I_{IA})[W_{IRA}\,W_{PRA} + (W_{IRA}^2 - W_{PRA}^2)\theta]$$

where:

$I_{(\ )}$ = moment of inertia of the float about each of its principal axes: pendulous axis (PA), input axis (IA), output axis (OA)

C_{OA} = the viscous damping coefficient about OA

P = the float pendulosity (ml)

$a_{(\ )}$ = the linear acceleration of the accelerometer along its respective axes: pendulous reference axis (PRA), input reference axis (IRA)

$W_{(\ )}$ = the angular velocity of case

θ = angle about OA of the float with respect to the case.

M_{TG} = commanded torque of the torque generator

The terms on the left correspond to the float dynamic response. The first two terms on the right correspond to the torque due to accelerometer input axis acceleration response and the accelerometer control torque. The remaining terms

represent the dynamic error torques; i.e.,

$$Pa_{PRA}\theta \text{- Cross Coupling}$$

$$I_{OA}\dot{W}_{ORA} \text{ - Output Axis Coupling}$$

$$(I_{PA} - I_{IA})[W_{IRA}W_{PRA} + (W_{IRA}^2 - W_{PRA}^2)\theta] \text{ - Anisoinertia}$$

Other terms could have been introduced had one considered additional misalignments of the float about the input and pendulous axes. They have been omitted so that a simple representation could be shown that would clearly evidence the nature of the desired error terms.

ANISOINERTIA ERROR- This term results from a difference in the float moment of inertia about IA and about PA. The applicable error expression is:

$$\text{Anisoinertia Error} = (I_{PA} - I_{IA})[W_{IRA}W_{PRA} + (W_{IRA}^2 - W_{PRA}^2)\theta] \tag{4.3}$$

This equation can be simplified because the secondary terms

$$[(I_{PA} - I_{IA})(W_{IRA}^2 - W_{PRA}^2)\theta] \tag{4.4}$$

involving small misalignment angles (typically < 1 arc minute) are negligibly small. The resulting anisoinertia error expression becomes

$$\text{Anisoinertia Error} = (I_{PA} - I_{IA})W_{IRA}W_{PRA} \tag{4.5}$$

OA COUPLING ERROR- This error term is introduced by the inertia

of the float output axis. This effect can be viewed as the tendency of the float to remain at rest when the case is accelerated about the output axis. The applicable error term is:

$$\text{OA Coupling Error} = -I_{OA}\dot{W}_{ORA} \qquad (4.6)$$

For constant output axis rate inputs and steady state oscillating environments the resulting error is zero.

SECTION 5

TEST MECHANIZATION AND PROCEDURES

DYNAMIC TEST FACILITY

The dynamic test facility consisted of a two-axis Leitz dividing head mounted on a gyro rate table and a test instrument console adapted for this program. A block diagram illustrating the functional elements of the controls, various test monitors and support equipment is shown in Fig. 5.1. Figure 5.2 shows the accelerometer and dividing head on the rate table. For the OA coupling test the gyro rate table was converted to a single axis angular oscillator. The dividing head was removed, and the accelerometer was mounted directly to the rate table.

An oven was built around the 2401 accelerometer for temperature control of the instrument. Although the PTSA loop should also have been temperature controlled, it was difficult to do so, due to its bulkiness and the limited time allotted to the test program. It is felt that, had the PTSA been temperature controlled, the uncertainties in the test results could have been reduced by an order of magnitude.

The interconnection of the accelerometer with the supporting electronics and test equipment was carefully developed to assure that noise on the signal generator and torquer lines where minimized. To eliminate ground loop problems, a single-point grounding scheme was employed. Lead lengths were minimized and critical signal lines were shielded to assure a minimum of pick-up. Input power was regulated to minimize power line transient effects on the accelerometer performance data.

Temperature errors due to the PTSA-accelerometer loop were kept to a minimum by controlling the laboratory temperature environment to 72 $\pm$ 2° F.

SECTION 6

TEST RESULTS

The tests run on the 2401 accelerometer are described in this section. The measurements included:

a) Determination of instrument scale factor (SF) and acceleration bias (A_b).

b) Anisoinertia measurement

c) OA coupling measurement

6.1 SCALE FACTOR AND ACCELERATION BIAS

Fundamental to accelerometer testing is the orientation of the instrument with regard to the local gravity vector. With the instrument input axis aligned for a positive one-g input, the relationship between the number of data pulses accumulated for a selected number of clock pulses is

$$SF\left(\frac{2P_1 - T}{T}\right) = g + A_b \qquad (6.1)$$

where:

SF = the positive scale factor constant corresponding to the magnitude of the incremental velocity represented

by each data pulse for +IA aligned parallel to the g vector.

A = the accelerometer bias expressed in the same dimensions as the gravity term 'g'.

P_1 = the number of data pulses accumulated during the preset count period in the +1g orientation.

P_2 = the number of data pulses accumulated during the preset count period in the -1g orientation.

T = the clock frequency times the counter preset.

g = local acceleration of gravity (980.4 cm/sec^2).

If the instrument input axis is aligned in a negative sense with respect to the local g vector, the corresponding equation is

$$SF\left(\frac{-2P_2 - T}{T}\right) = g - A_b \qquad (6.2)$$

By adding Eq. 6.1 and Eq. 6.2 and solving for scale factor SF we have

$$SF = \frac{g}{\frac{P_1}{T} - \frac{P_2}{T}} \quad cm/sec^2 \qquad (6.3)$$

The accelerometer bias can be determined by subtracting Eq. 6.2 from Eq. 6.1, resulting in the expression

$$A_b = SF\left(\frac{P_1}{T} + \frac{P_2}{T} - 1\right) \quad cm/sec^2 \qquad (6.4)$$

For the instrument under test, the following values were ascertained for SF and A_b

$$SF = 21121.1 \text{ cm/sec}^2$$

$$A_b = 18.7 \text{ cm/sec}^2$$

Test uncertainties of 0.3 cm/sec^2 were observed during the test.

6.2 ANISOINERTIA MEASUREMENT

The initial approach used to measure anisoinertia was to model the geometry of the test set up so that centripetal errors could be analytically compensated. However, since the rate table axis of rotation did not intersect and was not normal to the dividing head axis of rotation, no simple model could be obtained which would allow accurate compensation.

The second approach was to reduce the centripetal inputs to near zero by positioning the accelerometer center of gravity at the center of rotation of the rate table. Thus, any slight variation in geometry from an assumed ideal could contribute only negligibly small errors.

In the revised test setup, the accelerometer was mounted on the dividing head such that the input and pendulous axes

could be rotated in a vertical plane about the output axis. The dividing head was placed on the rate table such that the accelerometer did not sense any centripetal acceleration input. The accelerometer IA was positioned at eight positions relative to the gravity vector separated by 45° increments. The rate table was rotated at rates of 0.05 rad/sec and 1.0 rad/sec for each accelerometer position. The accelerometer output was recorded and the indicated error due to anisoinertia was calculated for each position using Eq. 6.5. See Fig. 6.1 and Fig. 6.2.

$$\text{Indicated Anisoinertia Error} = A_{IN}\text{at 1.0 rad/sec} - A_{IN}\text{at 0.05 rad/sec} \qquad (6.5)$$

Table 6.1 lists the results.

As can be seen from the tabulated results, the error term agrees with theory in that it should be zero at IA horizontal (180 and 360 degrees) and IA vertical (90 and 270 degrees), and the magnitude should be constant but change sign in accordance with the sign of the $W_{IA} W_{PA}$ product at the different 45° positions. Slight deviations from an ideal model are due to test uncertainties.

Since the primary anisoinertia term influencing the response of the accelerometer is $(I_{PA} - I_{IA}) W_{IA} W_{PA}$

the anisoinertia, $I_{PA}-I_{IA}$ can be calculated by averaging the results. Thus, for the table rate of 1.0 rad/sec and with the accelerometer IA set at a 45° angle from horizontal,

$$W_{IA}=W_{PA} = 0.7 \text{ rad/sec}$$

and

$$(I_{PA}-I_{IA}) W_{IA} W_{PA} = 1.47 \text{ cm/sec}^2$$

Thus, an anisoinertia error coefficient can be defined equal to, $I_{PA}-I_{IA}$ /ml, which for the 2401 accelerometer equals 3.0 cm. Also, since ml=1.12 gm-cm the corresponding anisoinertia is 3.4 gm-cm^2

6.3 OA COUPLING MEASUREMENT

The dynamic test facility was used for the OA coupling measurement. This test facility consists of a single-axis angular oscillator and a PDP/8L minicomputer. A block diagram illustrating the functional elements is shown in Fig. 6.3.

The accelerometer was mounted directly to the test table with its output axis aligned perpendicular to the table. Thus, an OA coupling input could be applied to the accelerometer

(input oscillations about the output axis) when the table was oscillated over a range of frequencies. The net output should have been zero, since theoretically there is no rectified torque due to oscillations about the output axis.

The accelerometer was oscillated over a range of frequencies from 1.0 to 100 HZ with amplitudes as shown in Table 6.2. For each input condition

$$(A_{in})_{\text{steady state}} = g\theta + A_b$$

was determined and compared to $(A_{in})_{ref.}$ determined at zero input (no oscillation of table).

The test was repeated with the table top rotated 90° about the tilt axis (IA up).

Tables 6.2 and 6.3 show the steady state accelerometer outputs with corresponding frequencies and amplitudes of oscillation.

The output distribution lies within the test uncertainty, indicating no definable OA coupling error.

SECTION 7

CONCLUSIONS AND RECOMENDATIONS

7.1 CONCLUSIONS

The following conclusions resulted from the dynamic test program.

1.) In order to get an accurate measurement of the anisoinertia error term, the test setup should not introduce any centripetal acceleration inputs.

2.) The measured anisoinertia error coefficient was 3.0 cm.

3.) It was confirmed that no rectified OA coupling error was present. Thus, the dynamic test results from this instrument confirm the theoretical predictions for a pendulous accelerometer.

4.) A bias uncertainty of 0.3 cm/sec^2 observed was possibly due to room temperature variation effects on the PTSA, superimposed on random noise and

errors introducei by short term averaging of data.

7.2 RECOMMENDATIONS

Any further testing of this instrument for small error coefficients should be done with a temperature controlled PTSA, since the accuracy of the test results might be limited by the lack of PTSA temperature control.

It is recommended that further dynamic tests be run with this instrument to establish the magnitude of the remaining dynamic error terms. These tests will require a two axis angular shaker and will establish a magnitude for the following:

1. Vibropendulosity
2. Anisoelasticity
3. Sculling

A discussion of these dynamic error terms and a corresponding test plan are contained in Appendix A.

REFERENCES

1. Knapp, P. J., Product Specification, Single Axis Viscous Damped Linear Accelerometer Part No. C702401030-1, Singer-Kearfott Division, August 17, 1970.

2. Bukow, G., Generalized PIPA Dynamics, M.I.T. Draper Laboratory ISS Memo 72-36, February 29, 1972.

3. Bukow, G., SIRU PIPA Module Dynamic Test, M.I.T. Draper Laboratory Proposal 70-169, June 9, 1970.

4. Sinkiewicz, J. S., Feldman, J., Lory, C. B., Evaluation of Selected Strapdown Inertial Instruments and Pulse Torque Loops, C. S. Draper Laboratory Report R-826, July 1974.

5. Gilmore, J. P., et al, Control, Guidance, and Navigation for Advanced Manned Missions, Vol. IV, Inertial Subsystems C. S. Draper Laboratory Report R-600, January 1968.

6. Lory, C. B., Feldman, J., Sinkiewicz, J. S., Dynamic Single-Degree-of-Freedom Integrating Gyroscope Used

in a Testing of a Single-Degree-of-Freedom Strapdown Gyroscope, C. S. Draper Laboratory Report E-2618, October 1971.

7. Wheaton, G. M., Strapdown Systems and Components-Test
8. Schneider, G. E., Studies on Dynamic Testing of a Strapped-Down Environment, M. S. Thesis, M.I.T. Department of Mechanical Engineering, Instrumentation Laboratory Report T-526, II, January 1967. Procedures, MIT Instramentation Laboratory Report E-2063 Vol. January 1970.

9. Lawrence, A. W., et al, The Design of an Advanced Strapdown Gyroscope, United Aircraft-Hamilton Standard Systems Center Division, February 15, 1970.

10. Groff, J. D., Operating Instructions for Single Axis Gyro Testing Electronics, United Aircraft-Hamilton Standard Systems Center Division, December 13, 1971.

APPENDIX A

MULTI-AXIS TEST PLAN PROPOSAL

The following test plan is derived from references 2 and 3. It presents a method for evaluating the dynamic accelercmeter response in the presence of vibration and rotating inputs. The following dynamic characteristics will be determined using a two-axis oscillator

1. Vibropendulous effect
2. Anisoelastic effect
3. Sculling

A.1 VIBROPENDULOUS EFFECT

When in-phase linear vibrations are applied along the input and pendulous axes of an undamped pendulous accelerometer a rectification of the vibration input occurs. For the case shown in Fig. A.1, the acceleration component along the input axis causes a rotation of the pendulum from its null position. A component of pendulosity thus exists along the reference IA direction and is sensitive to an acceleration input along the pendulous axis. When the vibration input reverses sign, a reversal in both the pendulum displacement, θ , and the

direction of the input acceleration along the pendulous axis maintains the sign of the sensed input and a rectified output results.

Assume that an input vibration a_{in} sinwt, is applied at an angle ψ relative to the pendulum input axis in the IA - PA plane. Assume also that the pendulum moves during a negligibly small time interval to the effective threshold of the rebalance loop employed. The rectified error is equivalent to

$$a_\epsilon = K_{IP}\, a_{in}^2 \cos\psi \sin\psi \sin^2\omega t \qquad (A.1)$$

$$= \frac{K_{IP}\, a_{in}^2}{2} \sin 2\psi \left[\frac{1 - \cos 2\omega t}{2}\right]$$

where: K_{IP} = the input axis-pendulous axis cross-coupling coefficient.

The steady state error peaks for $\psi = 45^\circ$. In addition to the DC component, there exists a sinusoidally varing term having a frequency equal to twice that of the vibration input.

For a vibropendulosity error to occur in a damped instrument, the inputs along the input axis and the pendulous axis must be out-of-phase. This is true because the float motion, due to the damping, will lag the phase of input along the input axis.

The instrument set-up for determining the vibropendulous

error is shown in Figure A.2. The accelerometer input axis lies parallel to the oscillator Y-axis. The pendulous axis lies parallel to the oscillator Z-axis. For low input frequencies, the pendulum will track the resulting vibration input along the input axis due to the Z-axis oscillation. Due to the fluid damping, the pendulum response will lag the driving input by almost 90°. Thus, the input along the pendulous axis (due to the Y-axis oscillation) must lag the first input by the same amount (X) to produce a rectified error output.

The instrument threshold will not have appreciable effect on the output obtained from the two simultaneous inputs. This will be true because only one term in the equation for the float response to a single vibratory input results in a rectified output in the presence of an input along the pendulous axis. This term is the sinusoidal response to the single axis vibratory input. The other terms in the complete response equation describe slow drifting of the float, or transients associated with the torquing pulses.

A.2 ANISOELASTIC EFFECT

In-phase linear vibrations along the input and output axes of an accelerometer can give rise to rectified error torques if unequal spring restraints exist along the input axis at opposite ends of the float. Fig. A.3 shows a representation

of a float with hypothetical positions for the center of gravity, center of floatation, and center of suspension. Under the action of an input acceleration, the following equilibrium equation results

$$(m_f a_{IA}) d_1 - m_{fl} a_{IA} d_2 + \Delta f_s d_s = 0 \qquad (A.2)$$

where:

m_f = mass of the float (grams)

m_{fl} = mass of the displaced fluid (grams)

d_1 = separation between the center of mass of the float and the suspension center (cm)

d_2 = separation between the center of floatation and the suspension center (cm)

Δf_s = difference between suspension restraining forces on opposite ends of the float (dyne)

d_s = separation between suspension forces (cm)

a_{IA} = input acceleration (cm/sec^2)

Examining the equation, if $m_f = m_{fl}$ (perfect flotation)

$$\Delta f_s = \frac{m_f a_{IA} (d_2 - d_1)}{d_s} \qquad (A.3)$$

If the pendulous member is unfloated, the buoyancy torque is absent and

$$\Delta f_s = \frac{m_f \, a_{IA} \, d_1}{d_s} \tag{A.4}$$

Defining K_s as the suspension stiffness, the rotation of the pendulous element, θ_R, corresponding to Δf_s is

$$\theta_R = \frac{\Delta f_s}{K_s \, d_s} \tag{A.5}$$

For the case of the perfectly floated instrument

$$\theta_{Rf} = \frac{m_f \, a_{IA} (d_2 - d_1)}{K_s \, d_s^2} \tag{A.6}$$

If simultaneous vibration inputs are applied to the accelerometer along both the input and output axes, an error analogous to that for the vibropendulous effect may be derived

$$E_{anisoelastic} = \frac{m_f (d_2 - d_1)}{2K_s \, d_s^2} \, a_{in}^2 \quad \text{for the steady state error} \tag{A.7}$$

The key terms in the equation are $(d_2 - d_1)$ and K_S. Good design will normally result in a value for $(d_2 - d_1)$ which approaches zero. The larger K_S is, the smaller the error that results.

The setup for determination of the anisoelastic effect is shown in Figure A.4. Here the oscillating inputs are applied

along the input and output axes. Again the threshold will have no effect on the results.

A.3 SCULLING

The phenomenon known as sculling occurs if simultaneous angular oscillation about the output axis and linear vibration along the pendulous axis are applied to the accelerometer. The applicable error term is

$$\text{Sculling Error} = K_{\alpha p} \frac{d W_{OA}}{dt} a_{PA} \tag{A.8}$$

The interaction torque term represents the sculling effect. Letting

$$\frac{d W_{OA}}{dt} = \alpha_m \sin bt \tag{A.9}$$

and

$$a_{PA} = +a_m \sin bt \tag{A.10}$$

$$\text{the Sculling Error} = +K_{\alpha p} \alpha_m a_m \sin^2 bt$$

$$= \frac{K_{\alpha p} \alpha_m a_m}{2} (1 - \cos 2bt) \tag{A.11}$$

Once again the reaction torque contains a rectified component and a sinusoidal component varying at twice the input frequency.

Figure A.5 shows the setup for the determination of the sculling effect. An OA coupling input is applied about the Z-axis. The Y axis oscillation provides an oscillating input along the pendulous axis.

Table 2.1

Kearfott 2401 Accelerometer - Performance Characteristics[1]

CHARACTERISTIC	SPECIFICATION	TOLERANCE	DIMENSIONS
Pendulum			
Pendulosity	1100	±15%	dyn-cm/g
Mechanical Freedom of Pendulum with Respect to the Case	±2	Minimum	mrad
Output Moment of Intertia	14	±20%	dyn-cm-s^2
Flexure Spring Rate	1540	±40%	dyn-cm/rad
Flexure Spring Rate	1.4	±50%	g/rad
Pickoff			
Pickoff Scale Factor*	10	±20%	V rms/rad
Input Impedance	(175 + J98)	±25%	ohms
dc Resistance - Excitation Coil	160	±25%	ohms
Output Impedance*	(115 + J20)	±25%	ohms
dc Resistance-Pickoff Coil	58	±25%	ohms
Electrical Quadrature Null (Trimmed)	200	Maximum	μV
Phase Angle*	(0)	±10	deg
Torquer			
Current Scale Factor	.99	±0.03	ma/g
Torquer Time Constant (T_2)	0.2 to 20	----	μs
dc Resistance - Torquer Coil	160	±25%	ohms
Damping			
Damping Coefficient	76,400	±40%	dyn-cm-s

* With external .2 mfd shunting capacitor.

(1) As published by Singer-Kearfott Division (Ref. 1)

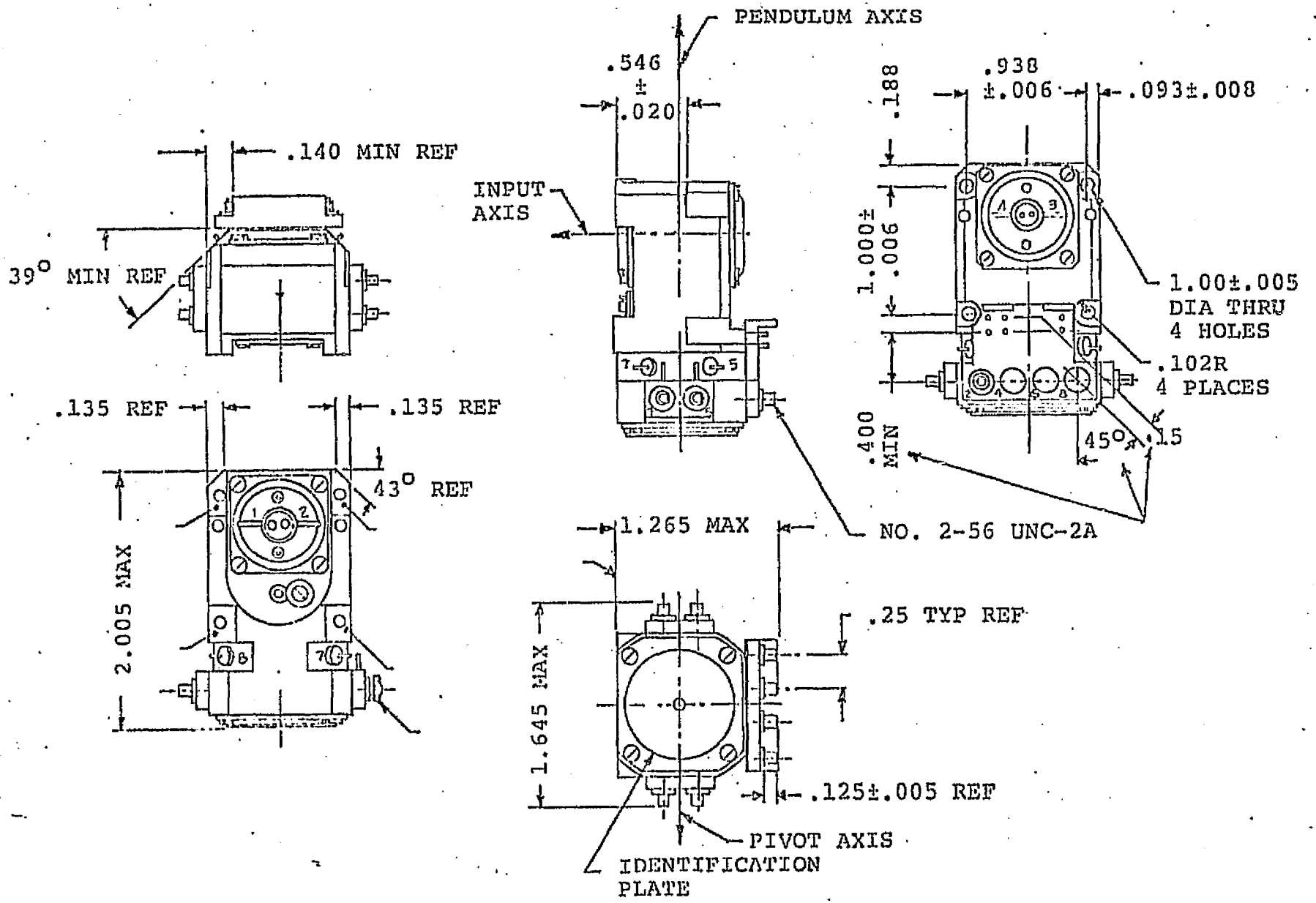

Fig. 2.1 Kearfott 2401 Accelerometer - Outline Dimensions

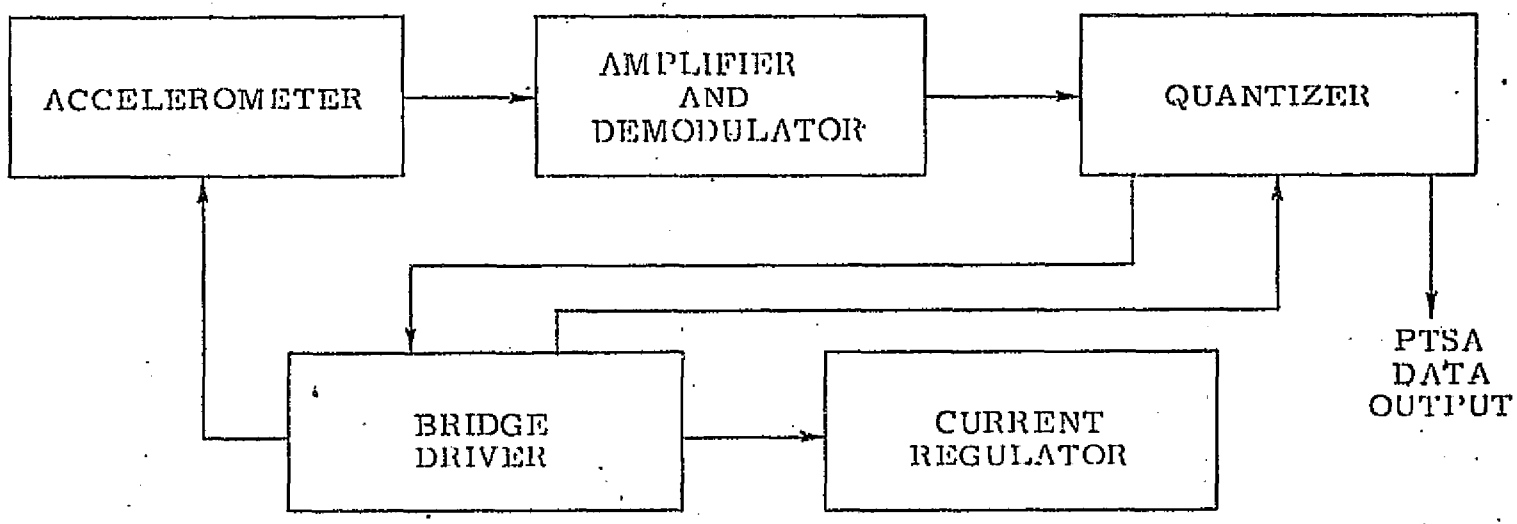

Fig. 3.1 Accelerometer / PTSA Block Diagram

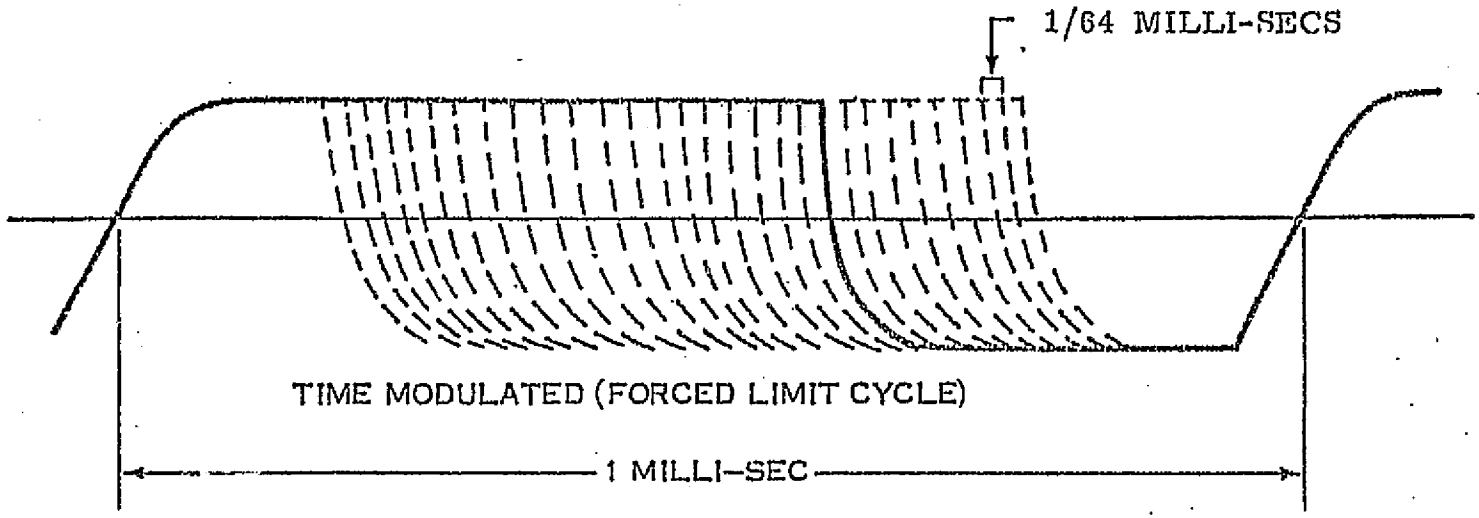

Fig. 3.2 Pulse Torquing Waveforms

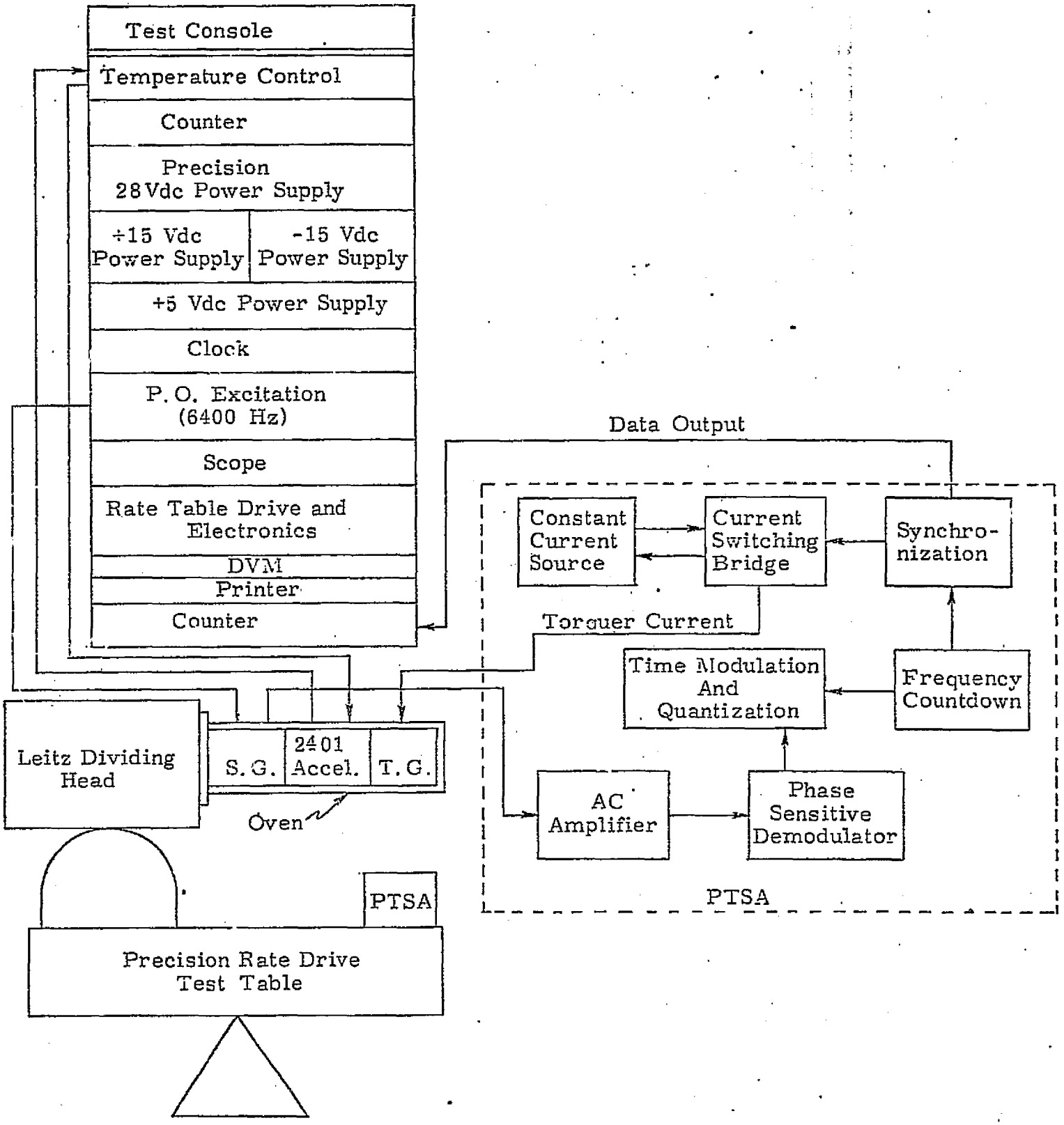

Fig. 5.1 Accelerometer, PTSA and Test Equipment

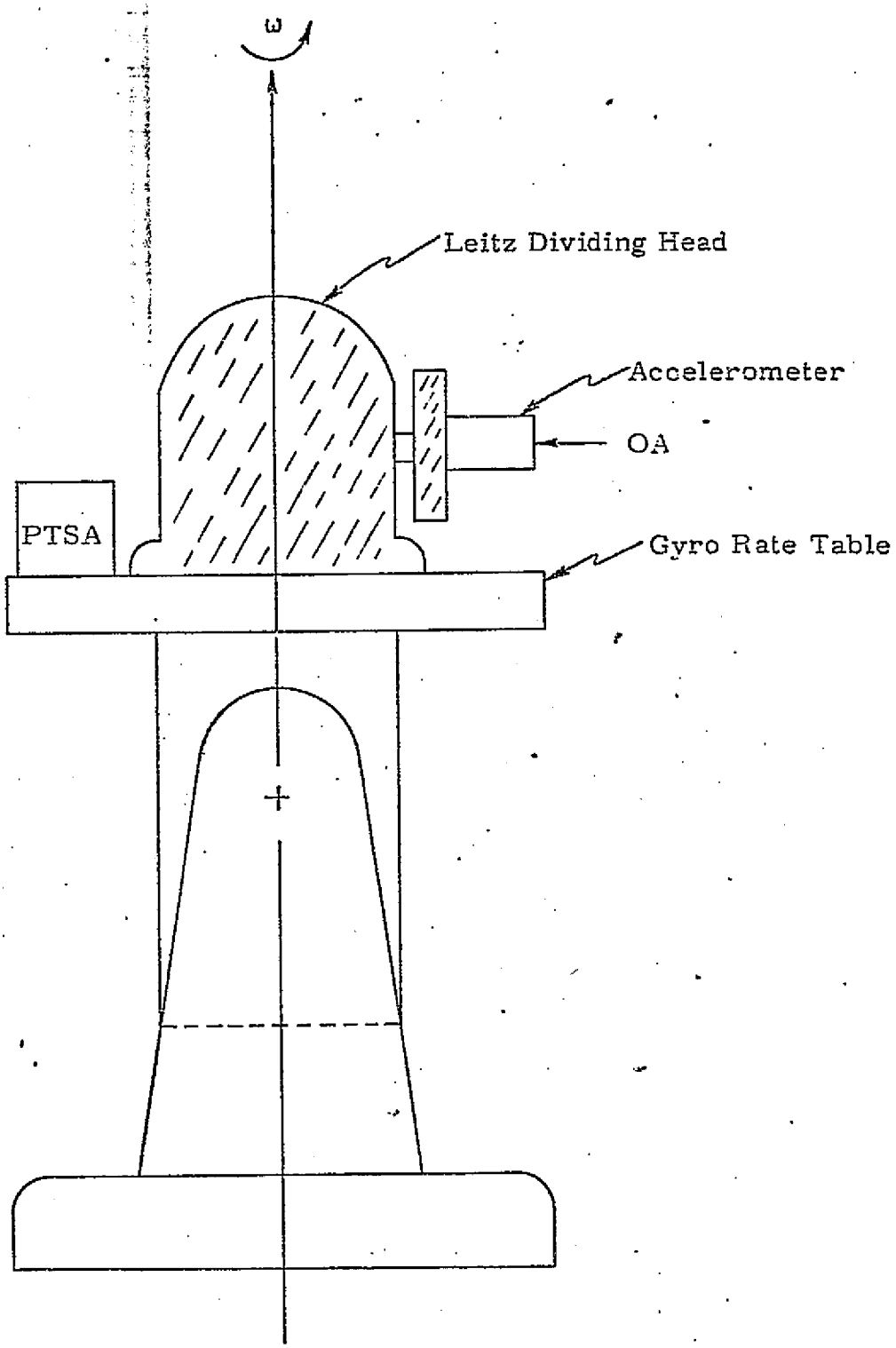

Fig. 5.2 Accelerometer Test Setup

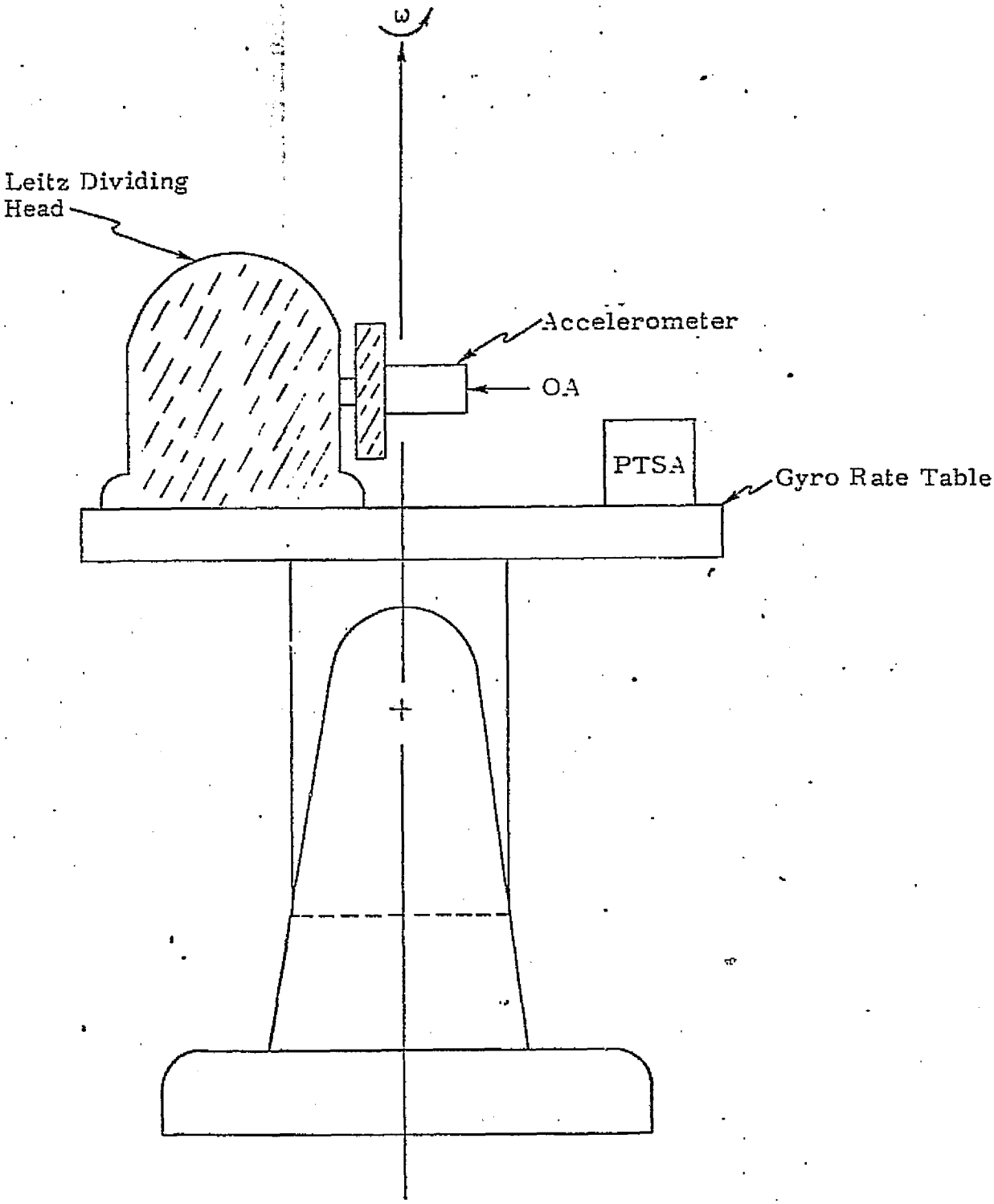

Fig. 6.1 Anisoinertia Test Setup

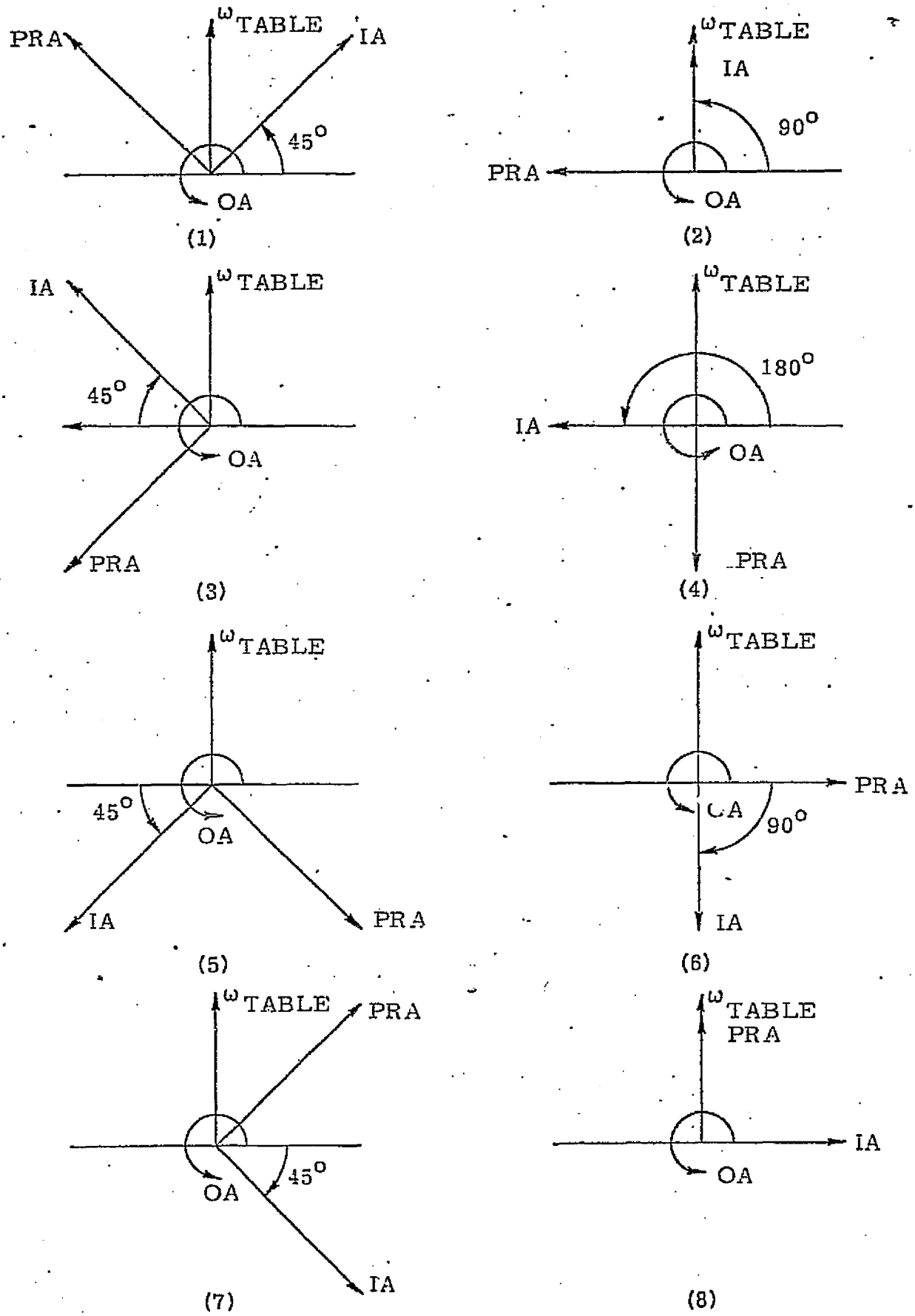

Fig. 6.2 Anisoinertia Test - IA Test Positions

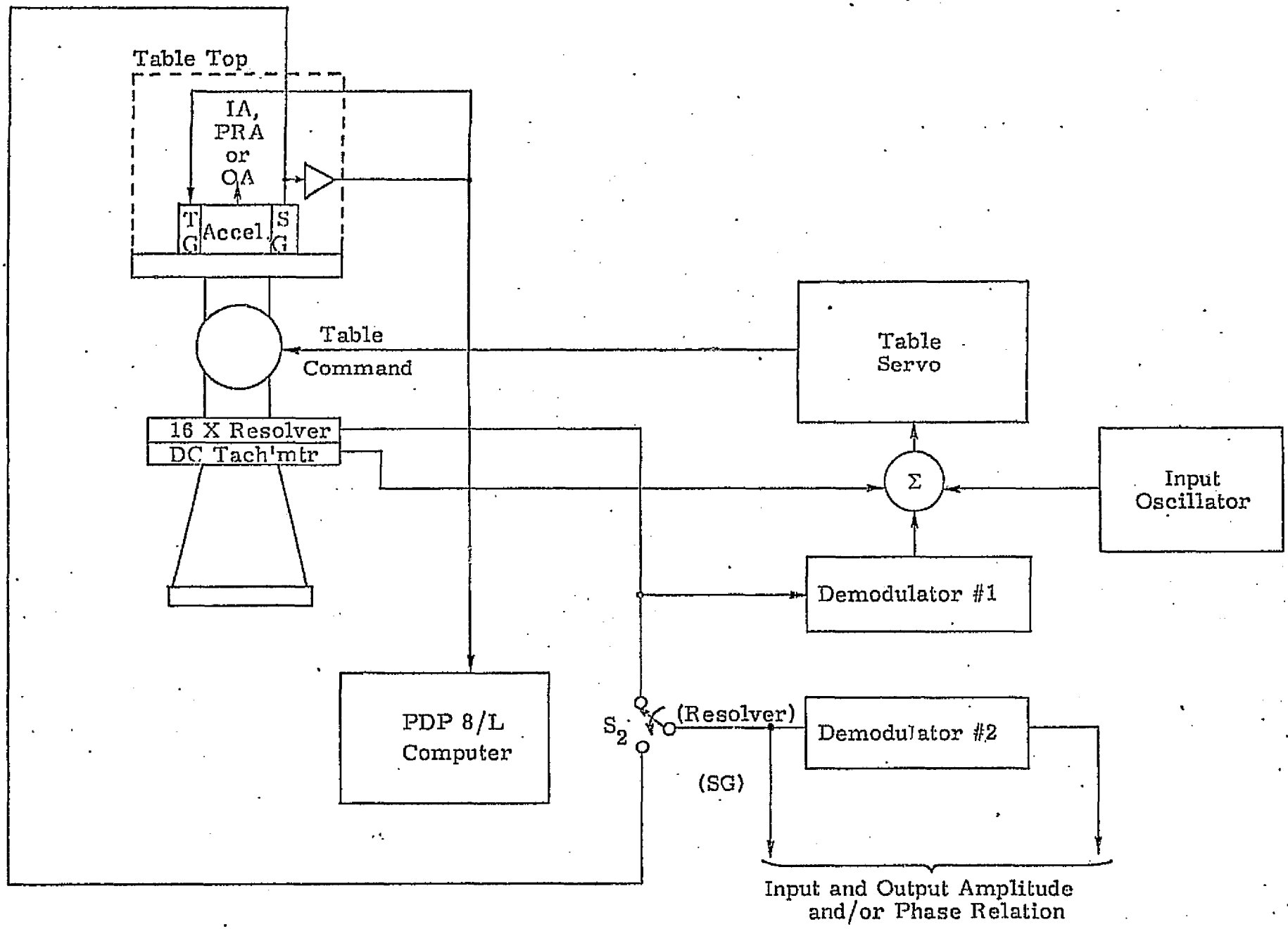

Fig. 6.3 Single Axis Oscillator

Table 6.1

Error Due to Anisoinertia

IA (degrees)	A_{in} (cm/sec^2)
45	1.54
90	0.07
135	-1.50
180	-0.32
225	1.54
270	0.31
315	-1.30
360	0.10

Table 6.2

OA Coupling Test Output
IA Horizontal

Frequency (Hz)	Amplitude (mr)	Static-Dynamic Output Difference (cm/sec^2)	
1	2.6	-0.03	
2	4.4	-0.07	
5	---	----	System Resonance
7.5	---	----	
10	---	----	
15	4.0	0.08	
20	2.0	0.25	
30	1.0	-0.21	
50	0.2	0.31	
60	0.1	-0.01	
75	0.1	0.19	
100	0.1	0.17	

Table 6.3

OA Coupling Test Output
IA Vertical

Frequency (Hz)	Amplitude (mr)	Static-Dynamic Output Difference (cm/sec^2)	
1	9.0	0.05	
2	---	----	System Resonance
5	---	----	System Resonance
10	10.0	0.10	
15	3.3	0.17	
20	2.0	0.31	
30	1.0	0.02	
50	0.2	0.01	
70	0.1	-0.14	
100	0.1	-0.13	

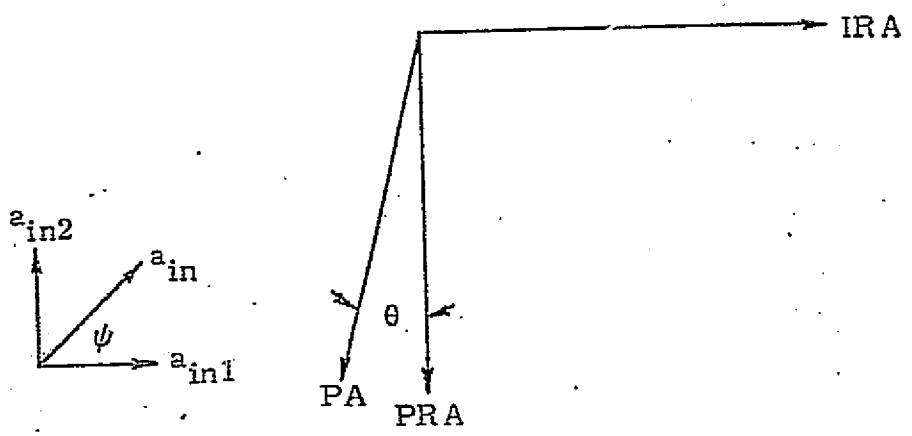

Fig. A.1 Vector Diagram for Vibropendulous Effect

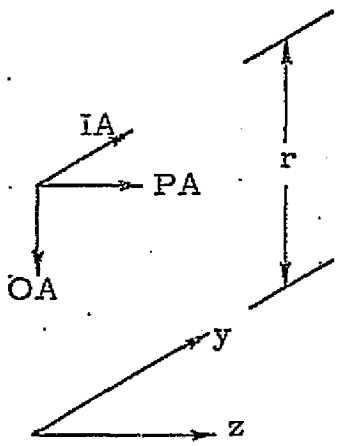

$\theta_y = \theta_{my} \sin(wt + \psi)$

$\theta_z = \theta_{mz} \sin wt$

$\psi \cong 90^o$

θ_{mo} = IA misalignment about OA

θ_{mp} = IA misalignment about PA

$\dot{\theta}_y = \theta_{my} w \cos(wt + \psi)$

$\ddot{\theta}_y = -\theta_{my} w^2 \sin(wt + \psi)$

$\dot{\theta}_z = \theta_{mz} w \cos wt$

$\ddot{\theta}_z = -\theta_{mz} w^2 \sin wt$

1. Input) $_{IAy} = -\theta_{mo} r \theta_{my} w^2 \sin(wt + \psi)$
2. Input) $_{IAz} = r \theta_{mz} w^2 \sin wt$
3. Input) $_{PAy} = -r\theta_{my} w^2 \sin(wt + \psi)$
4. Input) $_{PAz} = -\theta_{mo} r \theta_{mz} w^2 \sin wt$
5. Input) $_{OAy} = -r (\theta_{my} w \cos(wt + \psi))^2$ (centripetal acceleration)
6. Input) $_{OAz} = -r (\theta_{mz} w \cos wt)^2$ (centripetal acceleration)

Fig. A. 2 Axis Orientation; Vibropendulous Effect

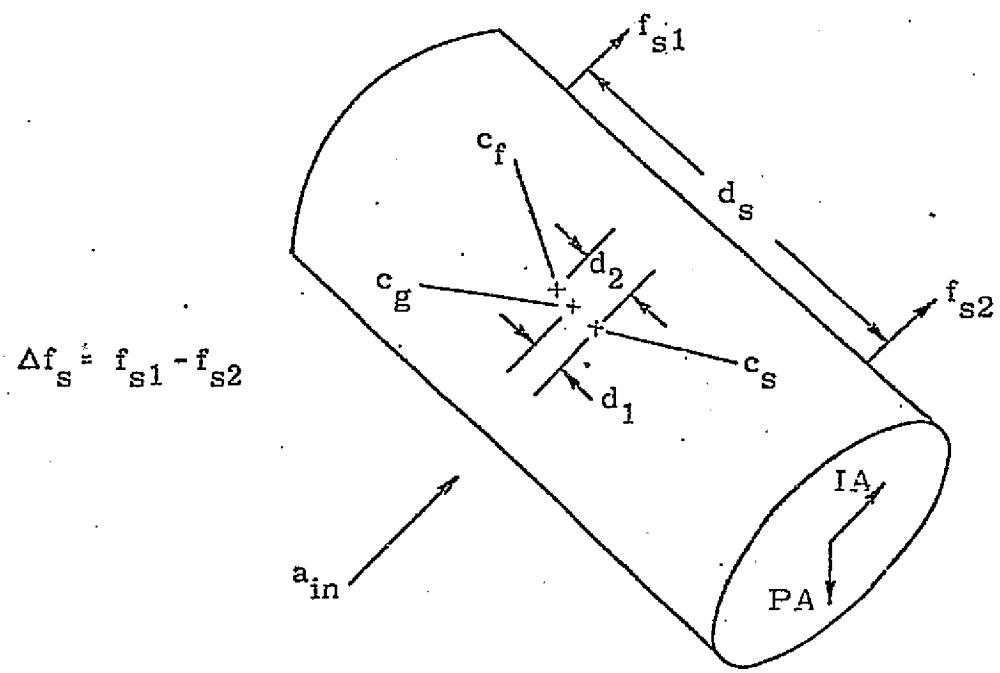

Fig. A.3 Force Diagram for Pendulous Float with Input Acceleration Along the Input Axis

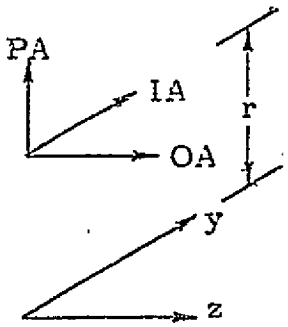

$$\theta_y = \theta_{my} \sin(wt + \psi)$$

$$\theta_z = \theta_{mz} \sin wt$$

$$\psi \cong 90^\circ$$

1. Input) $_{IAy} = -\theta_{mo}\, r\, \theta_{my}\, w^2 \sin(wt + \psi)$
2. Input) $_{IAz} = r\, \theta_{mz}\, w^2 \sin wt$
3. Input) $_{OAy} = -r\, \theta_{my}\, w^2 \sin(wt + \psi)$
4. Input) $_{OAz} = \theta_{mp}\, r\, \theta_{mz}\, w^2 \sin wt$
5. Input) $_{PAy} = -r\,(\theta_{my}\, w \cos(wt + \psi))^2$ (centripetal acceleration)
6. Input) $_{PAz} = -r\,(\theta_{mz}\, w \cos wt)^2$ (centripetal acceleration)

Fig. A.4 Axis Orientation: Anisoelastic Effect

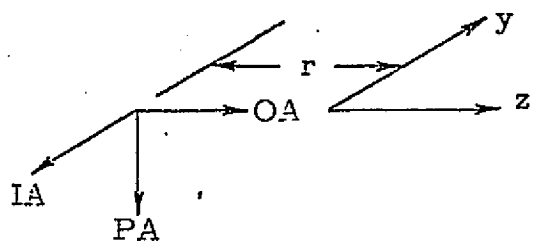

$$\theta_z = \theta_{mz} \sin wt$$

$$\theta_y = \theta_{my} \sin(wt + \psi)$$

$$\psi \cong 90^\circ$$

1. Input) $_{\text{about } OAz} = -\theta_{mz}\, w^2 \sin wt$
2. Input) $_{PAy} = r\, \theta_{my}\, w^2 \sin(wt + \psi)$
3. Input) $_{IAy} = \theta_{mo}\, r\, \theta_{my}\, w^2 \sin(wt + \psi)$
4. Input) $_{OAy} = -r\,(\theta_{my}\, w \cos wt)^2$ (centripetal acceleration)

Fig. A.5 Axis Orientation: Sculling